JOURNAL OF NATURAL PRODUCTS

pubs.acs.org/jnp

Article

Cannabinoids Block Cellular Entry of SARS-CoV-2 and the Emerging Variants

Richard B. van Breemen,* Ruth N. Muchiri, Timothy A. Bates, Jules B. Weinstein, Hans C. Leier, Scotland Farley, and Fikadu G. Tafesse

Cite This: https://doi.org/10.1021/acs.jnatprod.1c00946

Read Online

ACCESS | Metrics & More | Article Recommendations | Supporting Information

ABSTRACT: As a complement to vaccines, small-molecule therapeutic agents are needed to treat or prevent infections by severe acute respiratory syndrome coronavirus-2 (SARS-CoV-2) and its variants, which cause COVID-19. Affinity selection−mass spectrometry was used for the discovery of botanical ligands to the SARS-CoV-2 spike protein. Cannabinoid acids from hemp (*Cannabis sativa*) were found to be allosteric as well as orthosteric ligands with micromolar affinity for the spike protein. In follow-up virus neutralization assays, cannabigerolic acid and cannabidiolic acid prevented infection of human epithelial cells by a pseudovirus expressing the SARS-CoV-2 spike protein and prevented entry of live SARS-CoV-2 into cells. Importantly, cannabigerolic acid and cannabidiolic acid were equally effective against the SARS-CoV-2 alpha variant B.1.1.7 and the beta variant B.1.351. Orally bioavailable and with a long history of safe human use, these cannabinoids, isolated or in hemp extracts, have the potential to prevent as well as treat infection by SARS-CoV-2.

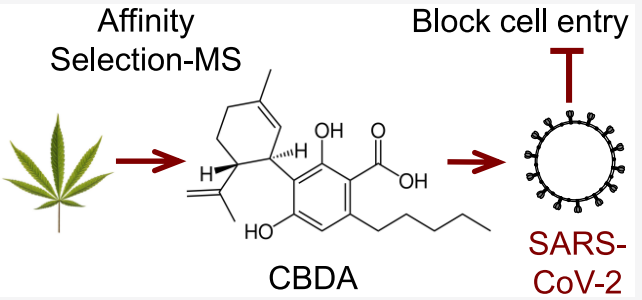

Caused by the severe acute respiratory syndrome coronavirus-2 (SARS-CoV-2), the COVID-19 pandemic includes at least 272 million cases worldwide, 5.3 million deaths, and over 600 000 new cases daily as of December 2021.[1] Vaccines have been developed, but due to their limited availability and the rate of virus mutation, SARS-CoV-2 infections are likely to continue for many years. As the pandemic continues, several SARS-CoV-2 variants have emerged that are circulating globally, including the variant B.1.1.7 (alpha, first detected in the United Kingdom), variant B.1.351 (beta, first detected in South Africa), and variant B.1.617.2 (delta, first detected in India).[2] These variants of concern are reported to have the capacity to escape humoral immunity elicited by natural infection or the current vaccinations. Moreover, the variants are associated with increases in infections and hospitalizations, suggesting a competitive fitness advantage over the original strain.[3]

A member of the Coronaviridae family, SARS-CoV-2 is an enveloped, nonsegmented, positive sense RNA virus that is characterized by crown-like spikes on the outer surface.[4,5] SARS-CoV-2 contains RNA strands 29.9 kb long[6] that encode the four main structural proteins, spike, envelope, membrane, and nucleocapsid, 16 nonstructural proteins, and several accessory proteins.[7] Any step of the SARS-CoV-2 virus infection and replication cycle is a potential target for antiviral intervention including cell entry, genome replication, viral maturation, or viral release. However, binding of the viral spike protein of SARS-CoV-2 to the human cell surface receptor angiotensin converting enzyme-2 (ACE2) is a critical step during the infection of human cells. Therefore, cell entry inhibitors could be used to prevent SARS-CoV-2 infection as well as to shorten the course of COVID-19 infections by preventing virus particles from infecting human cells.

A transmembrane protein with a molecular mass of ∼150 kDa, the spike protein forms homotrimers protruding from the SARS-CoV-2 surface. Subunits of the SARS-CoV-2 spike protein trimer consist of an S1 subunit that binds to ACE2 of the host cell to initiate infection, an S2 subunit that mediates virus fusion with host cells, and a transmembrane domain (Figure 1A). The infection of host cells by SARS-CoV-2 begins with the attachment of the receptor-binding domain (RBD) of the S1 protein,[8] which has been identified as residues 331 to 524,[9] to the host cell receptor ACE2. An enzyme on the outer cell membrane of host cells, ACE2 is expressed abundantly on human endothelial cells in the lungs, arteries, heart, kidney, and intestines.[10] TMPRSS2 protease on the host cell membrane activates the spike protein by cleaving it at S1/S2 and S2 sites,[11] leading to conformational changes that allow the virus to fuse with the host membrane and enter the

Received: October 3, 2021

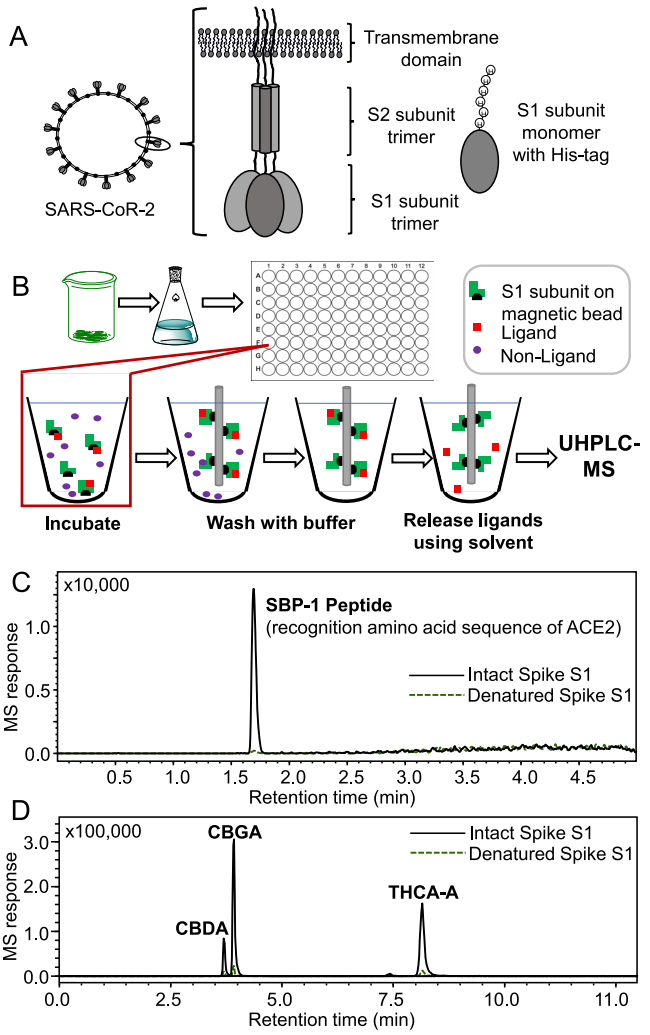

Figure 1. Affinity selection–mass spectrometric (AS-MS) discovery of natural ligands to the SARS-CoV-2 spike protein. (A) The spike protein of SARS-CoV-2 consists of trimers of a protein containing an S1 subunit, an S2 subunit, and a transmembrane domain. The S1 subunit binds to human ACE2 to initiate cell entry. Recombinant S1 containing a His-tag was immobilized on magnetic microbeads for affinity selection of ligands. (B) AS-MS was used to isolate and identify natural ligands to the spike protein S1 subunit. A magnetic probe retained the microbeads containing the S1 subunit and bound ligands, while unbound compounds were washed away. Ligands were released using organic solvent and then analyzed using UHPLC-MS. (C) During AS-MS, the SBP-1 peptide bound to immobilized S1 (equivalent to 0.17 μM) (positive control) but not to immobilized denatured S1 (negative control). (D) MagMASS was used for the affinity selection and identification of cannabinoid acids (0.10 μM each in this confirmatory chromatogram) as ligands from hemp extracts. Negative controls using denatured S1 showed no significant binding of cannabinoid acids.

cytoplasm. The S1 subunit is primarily responsible for the determination of the host virus range and cellular tropism.[12]

Ligands with high affinity to the receptor binding domain on the S1 protein have the potential to function as entry inhibitors and prevent infection of human cells by SARS-CoV-2.[13] For example, small peptides derived from the heptad repeat regions of SARS-CoV-1 spike S2 subunit have been shown to inhibit SARS-CoV infection by the interference of fusion with target cells.[14,15] The approach of utilizing compounds that block virus–receptor interaction has also been useful for other viruses, including HIV-1 and hepatitis C virus.[16,17]

Natural products are the most successful source of drugs and drug leads in the history of pharmacology.[18,19] Although combinatorial chemistry currently receives more emphasis for lead discovery by the pharmaceutical industry,[20] nature continues to be a source of unique chemical structural diversity for new drug discovery.[21] Approximately two-thirds of new small-molecule drugs since 1981 have been natural products, derivatives of natural products, natural product pharmacophores, or mimics of natural products.[18,22] Less than 10% of the world's biodiversity has been evaluated for potential biological activity, so that many more useful natural lead compounds await discovery.[18] As an example of a natural product with anti-SARS-CoV-2 activity, panduratin from the medicinal plant *Boesenbergia rotunda* was reported recently to be active against SARS-CoV-2 at both pre-entry and postinfection phases.[23]

Although bioassay-guided fractionation is widely used for natural products drug discovery, affinity selection–mass spectrometry (AS-MS) provides a more efficient alternative.[24] AS-MS involves incubating a therapeutically important receptor like the SARS-CoV-2 spike protein with a mixture of possible ligands such as a botanical extract. The ligand–receptor complexes are separated from nonbinding molecules using one of several methods such as ultrafiltration,[25] size exclusion,[26] or magnetic microbeads,[27] and then ultra-high-pressure liquid chromatography–mass spectrometry (UHPLC-MS) is used to characterize the affinity-extracted ligands. In this investigation, we used the AS-MS approach of magnetic microbead affinity selection screening (MagMASS).[28,29]

Hemp (*Cannabis sativa* L., Cannabaceae) is used for fiber, food, and animal feed, and various hemp extracts and compounds have become popular additions to cosmetics, body lotions, dietary supplements, and food. Over 170 secondary metabolites including some unique compounds are produced by hemp[30,31] including flavonoids, diterpenes, triterpenes, lignans, and cannabinoids. Orally bioavailable,[32] there are at least 70 cannabinoids including cannabidiols, Δ^9-tetrahydrocannabinols, Δ^8-tetrahydrocannabinols, cannabigerols, cannabinols, cannabichromenes, and cannabitriols, and in 2018, the U.S. FDA approved a cannabidiol isolate (Epidiolex), for the treatment of seizures associated with certain types of epileptic seizures.[33]

Using MagMASS to screen hemp extracts for ligands to the SARS-CoV-2 spike protein, several cannabinoid ligands were identified and ranked by affinity to the spike protein. Two cannabinoids with the highest affinities for the spike protein, cannabidiolic acid (CBDA) and cannabigerolic acid (CBGA), were confirmed to block infection of human epithelial cells by a pseudovirus expressing the spike protein. More importantly, both CBDA and CBGA block infection of the original live SARS-CoV-2 virus and variants of concern, including the B.1.1.7 and B.1.351.

RESULTS AND DISCUSSION

Discovery of Hemp Ligands against SARS-CoV-2. To discover natural ligands to the SARS-CoV-2 spike protein, a MagMASS[27] assay was developed using the spike protein S1 subunit immobilized on magnetic microbeads (Figure 1). To confirm that the immobilized S1 subunit retained selectivity for the human cell surface protein ACE2, magnetic microbeads containing the S1 subunit were incubated with SBP-1, which is

https://doi.org/10.1021/acs.jnatprod.1c00946
J. Nat. Prod. XXXX, XXX, XXX−XXX

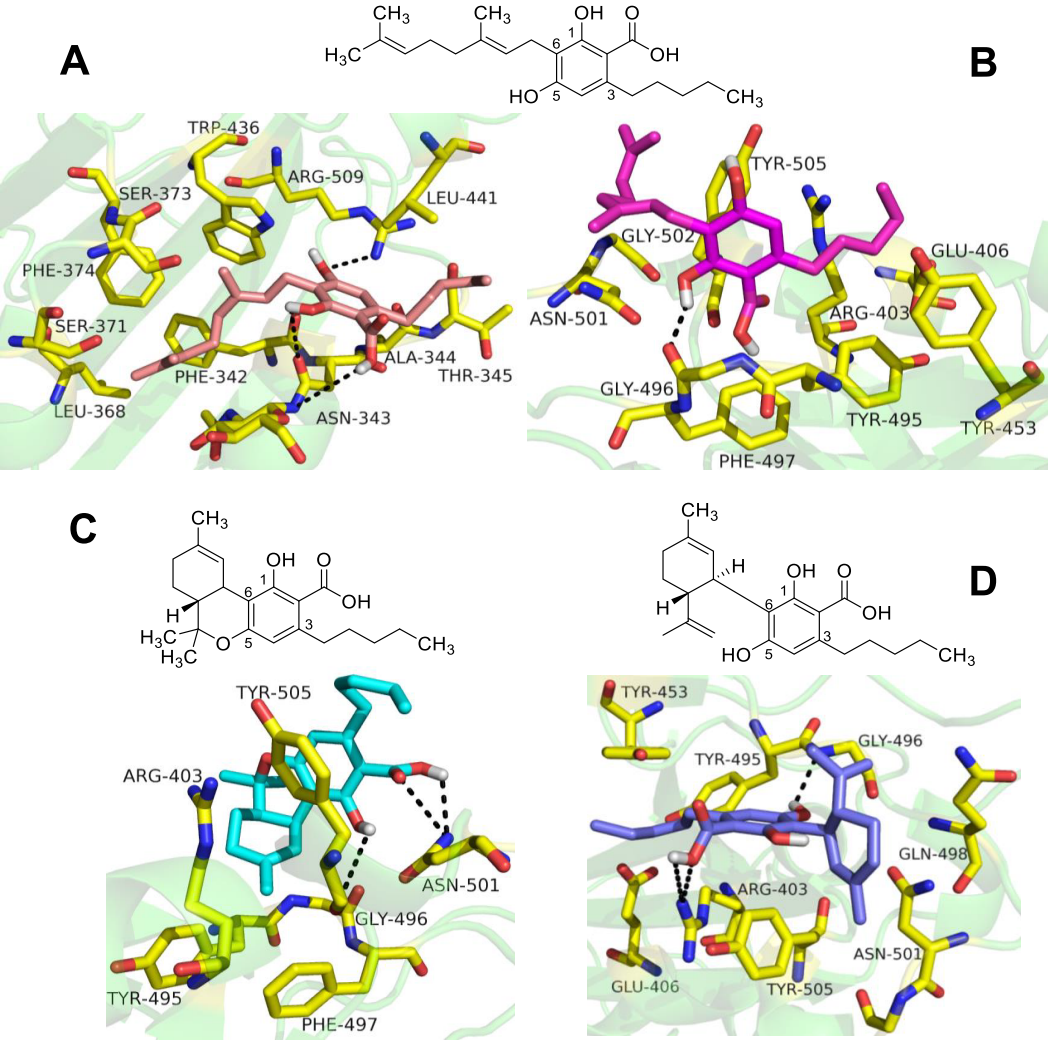

Figure 2. Computational based modeling of the binding of cannabinoid acids to the SARS-CoV-2 spike protein S1 C-terminal domain using AutoDock Vina. The active site residues of the S1 subunit are shown in yellow. (A) CBGA (pink) is predicted to bind to the anallosteric site (−6.6 kcal/mol free energy of binding). (B) Although less favorable (−6.2 kcal/mol), CBGA (magenta) can also bind to the orthosteric site on the S1 C-terminal domain. (C) THCA-A (cyan) and (D) CBDA (teal) are predicted to bind at the orthosteric site with free energies of binding of −6.5 kcal/mol and −6.3 kcal/mol, respectively.

a peptide containing the amino acid sequence of human ACE2 to which the SARS-CoV-2 virus spike protein recognition site binds (amino acid residues 331 to 524). After processing using MagMASS (Figure 1B), SBP-1 showed selective binding to the immobilized spike protein S1 subunit (positive control), whereas SBP-1 did not bind to the denatured S1 subunit that had been immobilized in an identical manner (Figure 1C).

During screening of botanical extracts using MagMASS, extracts of hemp (*C. sativa* L.) produced several hits (Figure 1D). Based on dereplication of the hits and follow-up assays using cannabinoid standards, the spike protein ligands with the highest affinities were identified as CBGA, tetrahydrocannabinolic acid (THCA-A), and CBDA (Figures 2−4, Supporting Information). The cannabinoids Δ^9-tetrahydrocannabinol, Δ^8-tetrahydrocannabinol, cannabichromene, cannabigerol, cannabinol, and cannabidiol showed only weak or no binding based on competitive binding MagMASS assays[34] using equimolar mixtures (Table 1).

Dissociation Constants and Ligand Docking. The K_d values for the binding of CBGA and CBDA to the SARS-CoV-2 spike protein S1 subunit were determined using equilibrium dialysis. The optimum time for full equilibration of CBGA was 5 h, while that of CBDA was 4 h. The K_d values for CBGA and CBDA were 19.8 ± 2.7 and 5.6 ± 2.2 μM, respectively. Because THCA-A is a controlled substance, insufficient quantities were available for determination of binding affinity or antiviral activity.

The binding interactions of CBDA, THCA-A, and CBGA with the SARS-CoV-2 spike protein S1 C-terminal domain were modeled using AutoDock Vina (Figure 2). In agreement with the MagMASS rank ordering of ligands (Table 1), the free energy of binding was greatest for CBGA (−6.6 kcal/mol) followed by THCA-A (−6.5 kcal/mol) and CBDA (−6.3 kcal/mol). The optimum binding mode for CBGA was at an allosteric site with a binding pocket dominated by hydrophobic residues within a van der Waals distance of 4 Å, namely, F374, L368, F342, W436, A344, and L441 (Figure 2A). The hydrophobic isoprenyl group of CBGA interacted with the hydrophobic residues L368, F342, F374, and W436, while the pentyl group interacted with A344, L441, and the amide of T345. The carboxylic acid group formed a hydrogen bond with the D343 amide side chain, while the hydroxy groups at

https://doi.org/10.1021/acs.jnatprod.1c00946
J. Nat. Prod. XXXX, XXX, XXX−XXX

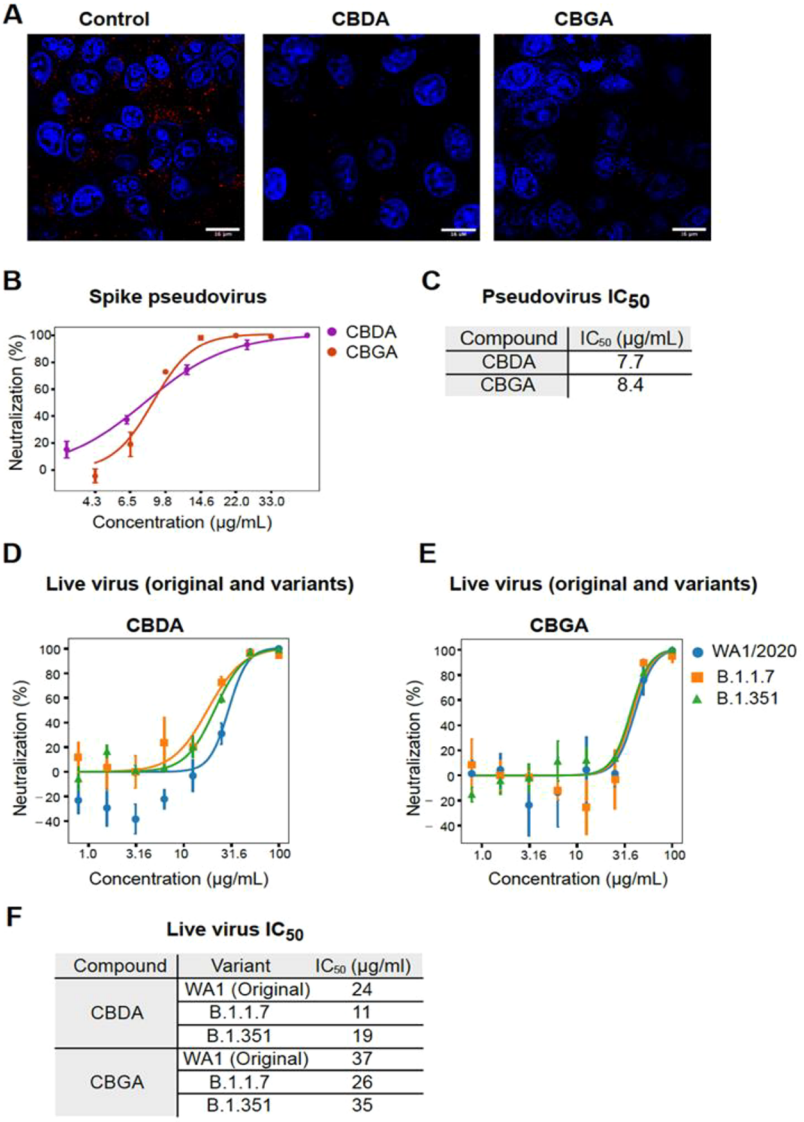

Figure 3. CBD compounds block viral entry of SARS-CoV-2 through spike binding. Neutralization of spike protein pseudotyped lentivirus and multiple variants of live SARS-CoV-2 virus by cannabinoids CBDA and CBGA. (A) Representative images of high-resolution microscopy of SARS-CoV-2 (WA1/2020)-infected Vero E6 cells treated with 25 μg/mL CBDA, CBGA, or vehicle (control). Cells were stained with anti-ds-RNA (red) antibody to visualize replication sites formed during infection. DAPI (blue) was used to stain nuclei. (B) Infection of ACE2 293T cells with SARS-CoV-2 spike pseudotyped lentivirus in the presence of CBDA or CBGA. Percent neutralization was determined by quantification of total GFP signal resulting from successful pseudovirus infection, normalized to vehicle control (n = 3). (C) Table of IC_{50} values for pseudovirus experiments. (D and E) Live-virus infection of Vero E6 cells with SARS-CoV-2 variants (WA1/2020, B.1.1.7, and B.1.351) in the presence of CBDA (D) or CBGA (E). Percent neutralization was normalized to vehicle control wells (n = 3). (F) Table of IC_{50} values for live-virus experiments shown in D and E. IC_{50} values were determined by fitting data to a three-parameter model for pseudotype infection (C) and live-infection (F) experiments.

positions 1 and 5 formed hydrogen bonds with the side chains of D343 and R509, respectively. Although less favorable, CBGA was also predicted to bind orthosterically to the spike protein S1 C-terminal domain with −6.2 kcal/mol free energy of binding (Figure 2B).

Unlike CBGA, CBDA and THCA-A were predicted to bind preferentially within the orthosteric site of the spike protein S1 subunit. The key interactions for CBDA include hydrogen bonding between the carboxylic acid group and the R403 side chain and hydrophobic interactions between the CBDA aromatic ring and the Y495 side chain (Figure 2C). Additional hydrophobic contributions were made by Y505, G496, and Y453. The hydroxy group at position 5 of CBDA formed a hydrogen bond with the amide group of G496. THCA-A was predicted to bind at the surface of the orthosteric site in a hydrophobic region consisting of Y495, F497, Y505, and G496 (Figure 2D). Hydrogen bond interactions could form between the carboxylic acid and D501 as well as between the hydroxy group at position 1 and the carbonyl group of Y505.

Inhibition of SARS-CoV-2 Cell Entry. To determine if CBDA or CBGA could prevent infection by blocking SARS-CoV-2 cell entry, pseudovirus and live SARS-CoV-2 virus cell infection assays were carried out. We incubated the live SARS-CoV-2 virus with 25 μg/mL of either CBDA, CBGA, or vehicle control (DMSO) and then infected Vero E6 cells. At 24 h postinfection, cells were stained with anti-double-stranded RNA (dsRNA) antibody known to bind specifically to viral RNA. We found an absence of SARS-CoV-2 viral RNA in cells treated with either cannabinoid (Figure 3A). To quantify the level of inhibition, we produced spike protein pseudotyped

https://doi.org/10.1021/acs.jnatprod.1c00946
J. Nat. Prod. XXXX, XXX, XXX−XXX

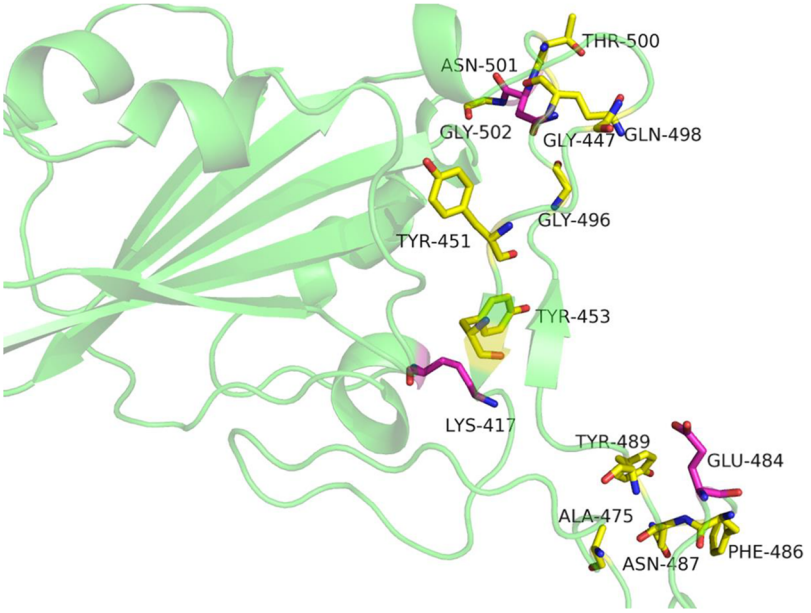

Figure 4. Orthosteric site residues of the spike S1 receptor binding domain. The residues in magenta are mutated in the B.1.351 variant (K417N, E484 K, N501Y). The B.1.1.7 variant mutation occurs at N501Y.

Table 1. MagMASS Ranking of Hemp Cannabinoids for Binding to the SARS-CoV-2 Spike Protein[a]

cannabinoid[b]	UHPLC retention time (min)	fold peak area enrichment[c]
cannabigerolic acid (CBGA)	3.8	20.5 ± 0.51
tetrahydrocannabinolic acid (THCA-A)	8.2	16.7 ± 2.2
cannabidiolic acid (CBDA)	3.7	12.2 ± 0.52
cannabinolic acid (CBNA)	6.5	5.6 ± 1.4
cannabigerol (CBG)	4.1	3.4 ± 0.82
cannabinol (CBN)	5.7	3.4 ± 0.78
Δ^8-tetrahydrocannabinol (Δ_8-THC)	6.8	3.1 ± 0.81
Δ^9-tetrahydrocannabinol (Δ_9-THC)	6.8	3.0 ± 0.77
cannabidiol (CBD)	4.2	2.9 ± 0.72
cannabichromene (CBC)	8.1	2.9 ± 0.75
Cannabidivarin (CBDV)	3.0	1.6 ± 0.17

[a]Mean ± SE (n = 3). [b]Equimolar cannabinoid mixture (0.10 μM) incubated with the S1 subunit of spike protein (0.17 μM). [c]Fold peak area enrichment = (UHPLC-MS/MS peak area experiment)/(UHPLC-MS/MS peak area negative control using denatured spike protein S1 subunit).

lentiviral particles with a GFP reporter gene, and HEK 293T cells overexpressing ACE-2 were infected for 48 h with these lentiviral particles following treatment with varying concentrations of CBDA, CBGA, or vehicle control. The number of infected cells was quantified by fluorescence microscopy, and the concentration that reduced pseudovirus infections by half (IC_{50}) was 7.7 μg/mL for CBDA and 8.4 μg/mL for CBGA (Figure 3B,C). The cytotoxicity of these compounds was insignificant at concentrations below 50 μg/mL for Caco2, 293T-ACE2, and Vero cell lines (Figure 4, Supporting Information).

To validate the virus neutralizing capabilities of CBDA and CBGA, we next performed focus forming assays using authentic SARS-CoV-2 virus (Isolate USA-WA1/2020). We utilized Vero E6 cells for these experiments due to their high susceptibility to the virus and common use in SARS-CoV-2 live-virus studies. Focus forming assays were performed using serial dilutions of CBDA or CBGA that were incubated with infectious SARS-CoV-2 for 1 h prior to infection. As in the pseudovirus neutralization assay, CBDA and CBGA prevented SARS-CoV-2 entry into Vero E6 cells with IC_{50} values of 24 and 37 μg/mL (Figure 3D−F), respectively.

Emerging variants of concern (VOC), including B.1.1.7 and B.1.351, have been shown to resist neutralization by antibodies generated against earlier lineages of SARS-CoV-2. To assess whether blockage of cell entry by CBDA and CBGA is variant dependent, we performed additional focus forming assays using the live SARS-CoV-2 variants B.1.1.7, containing the N501Y spike protein mutation, and B.1.351, containing the K417N, E484 K, and N501Y spike mutations. Like WA1/2020 infections, CBDA and CBGA both blocked B.1.1.7 infection with IC_{50} values of 11 and 26 μg/mL, respectively. B.1.351 was neutralized as well by both compounds with IC_{50} values of 19 and 37 μg/mL, respectively (Figure 3D−F), indicating no substantial loss of activity against these VOCs.

Originally invented for high-throughput screening of pools of combinatorial libraries,[35] the selectivity, sensitivity, and speed of AS-MS approaches like MagMASS are also ideal for screening natural products mixtures such as botanical extracts.[36] Compared with conventional high-throughput screening utilizing fluorescence or absorbance readouts (such as FRET or fluorescence polarization), AS-MS offers advantages such as compatibility with any type of ligand mixture, matrix, and assay buffer and no requirement for fluorescent tags. Uniquely, AS-MS does not suffer from interference from samples containing fluorophores or chromophores, which are common in natural products. One of the newer AS-MS techniques,[27,37] MagMASS offers advantages compared with the other AS-MS approaches that use ultrafiltration or size exclusion such as ease of automation and faster separation of receptor−ligand complexes from unbound compounds, which minimizes ligand loss due to premature dissociation from the receptor and maximizes

https://doi.org/10.1021/acs.jnatprod.1c00946
J. Nat. Prod. XXXX, XXX, XXX−XXX

sensitivity.[24] Therefore, MagMASS is an ideal platform for the discovery of natural ligands of the SARS-CoV-2 spike protein.

Recently, the crystal structure of the C-terminal domain of the SARS-CoV-2 spike protein in complex with the human ACE2 receptor was solved. The key interactions involve residues along the spike protein C-terminal domain interface that contribute to a network of hydrogen bonding and salt-bridge interactions with the ACE2 receptor. The residues on the spike protein involved in the binding to ACE2 include A475, N487, E484, Y453, K417, G446, Y449, G496, Q498, T500, G502, Y489, and F486. The interaction of the virus with the ACE2 receptor is mainly contributed by the polar interactions resulting from hydrophilic residues on the surface of the spike protein C-terminal domain.[38]

In the AutoDock Vina docking program, the ligand docking in the active site is based on algorithms that take into consideration the steric, hydrophobic bonding, and hydrogen bonding interactions between the ligand and active site residues. The best predicted binding conformation should have the lowest free energy of binding (kcal/mol). CBGA gave the lowest free energy of binding (−6.7 kcal/mol) to an allosteric site, with a root-mean-square deviation of 24.3 from the orthosteric site. On the other hand, THCA-A and CBDA had slightly higher energies of binding at −6.5 and −6.3 kcal/mol, respectively. Overall, the MagMASS data show that CBGA binds to the spike protein S1 subunit strongly in cannabinoid mixtures, suggesting that it binds allosterically and does not compete for binding with orthosteric cannabinoid ligands.

Variants of the SARS-CoV-2 virus such as B.1.1.7 and B.1.351 include amino acids in the spike protein S1 subunit that interact with the ACE2 receptor.[39] For example, the N501Y mutation was identified by bioinformatics analysis of data derived by metagenomics sequencing of samples obtained from a patient with persistent SARS-CoV-2 infection. Other highly infectious variants identified that include mutation of the active site residues include N501T, K417, and E484 K (Figure 4).[40] With the rapid mutations occurring, a novel inhibitor capable of binding to an orthosteric site would be of great interest in the intervention of SARS-CoV-2 variants characterized by active site mutations.

Our infection inhibition assay results clearly indicate that CBDA and CBGA are both able to block cell entry by SARS-CoV-2. The concentrations needed to block infection by 50% of viruses is high but might be clinically achievable. For example, CBDA administered orally to human volunteers at 0.063 mg/kg showed greater bioavailability than CBD and produced maximum plasma concentrations of 0.21 μM.[32] In beagle dogs, oral administration of CBDA at 1 mg/kg was well tolerated, was 2-fold more bioavailable than CBD, and produced serum levels up to 1.42 μM.[41] Although no data on the bioavailability of CBGA are yet available, the data for CBDA suggest that μM plasma and serum concentrations for CBGA should also be possible.

Previous reports have indicated that one possible mechanism for inhibition of SARS-CoV-2 by decarboxylated cannabidiol (CBD) is activation of innate immune mechanisms.[42] However, our live-virus data indicate that inhibition by CBDA and CBGA occurs at the point of cell entry. These mechanisms are not mutually exclusive, and it remains possible that multiple cannabinoids in complex mixtures from plant extracts could act independently to inhibit SARS-CoV-2, potentially leading to enhanced effectiveness when compared to individual compounds.

One of the primary concerns in the ongoing pandemic is the spread of viral variants, of which there are many, with some of the most concerning and widespread being B.1.1.7 and B.1.351. These variants are well known for evading antibodies against early lineage SARS-CoV-2, which is particularly concerning due to the fact that current vaccination strategies rely on the early lineage spike RBD as an antigen. Our data show minimal impact of the variant lineages on the effectiveness of CBDA and CBGA, a trend that will hopefully extends to other existing and future variants. Because we believe that the primary binding site for CBGA is allosteric, there may even be reduced evolutionary pressure for SARS-CoV-2 to mutate their binding sites compared to the orthosteric binding sites typically favored by neutralizing antibodies. With widespread use of cannabinoids, resistant variants could still arise, but the combination of vaccination and CBDA/CBGA treatment should create a more challenging environment with which SARS-CoV-2 must contend, reducing the likelihood of escape.

EXPERIMENTAL SECTION

General Experimental Procedures. Mass spectrometric analyses were carried out using a Shimadzu (Kyoto, Japan) Nexera UHPLC system interfaced with an LCMS-9030 Q-ToF hybrid high-resolution mass spectrometer or an LCMS-8050 triple quadrupole mass spectrometer.

Plant Material. Extracts of hemp and isolates of specific cannabinoids were obtained from the Global Hemp Innovation Center (Oregon State University, Corvallis, OR, USA). Plant taxonomy was confirmed by Jay S. Noller of the Global Hemp Innovation Center. Certified cannabinoid standards were purchased from Cayman Chemical (Ann Arbor, MI, USA).

Affinity Selection−Mass Spectrometry. Recombinant SARS-CoV-2 spike protein (RayBiotech; Peachtree Corners, GA, USA) (~72 kDa) containing an N-terminal His-tag was immobilized on Ni^{2+}-nitrilotriacetic acid-derivatized magnetic microbeads (EmerTher; Parsippany, NJ, USA) for use in the affinity selection−mass spectrometry approach MagMASS. As a negative control, denatured spike protein was immobilized on identical magnetic microbeads. The spike protein for the negative control incubations was denatured by incubating in a 95 °C water bath for 15 min. Positive control incubations used SBP-1 (RayBiotech), a 23 amino acid peptide with the sequence of IEEQAKTFLDKFNHEAEDLFYQS, which is identical to the ACE2 α1 helix sequence recognized by the SARS-CoV-2 spike protein. SBP-1 (33 nM) was incubated for 60 min with magnetic microbeads containing 50 pmol of immobilized active or denatured S1 protein in 300 μL of binding buffer. After washing twice with 500 μL of 30 mM ammonium acetate to remove unbound ligand while the beads were retained by a magnetic field, ligand was released from the beads using 90% methanol in water (200 μL) and analyzed using UHPLC-LC/MS. SBP-1 was measured using positive ion electrospray with selected reaction monitoring on a triple quadrupole mass spectrometer at unit resolution. For SBP-1, the selected reaction monitoring transitions were m/z 701.6 ($[M + 4H]^{4+}$) to m/z 136.2 (quantifier) and m/z 701.6 ($[M + 4H]^{4+}$) and m/z 120.2 (qualifier) at collision energies of −30 and −45 V, respectively, with a dwell time of 25 ms per transition.

Extracts (10 μg), mixtures of cannabinoid standards (0.10 μM each), or cannabinoid standards (0.10 μM) were incubated with 50 pmol of immobilized SARS-CoV-2 spike protein and screened using MagMASS as described above. The released ligand was analyzed using UHPLC-LC/MS with reversed phase UHPLC separation on a Waters (Milford, MA, USA) Acquity UPLC BEH C_{18} column (1.7 μm, 130 Å, 2.1 mm × 50 mm) with a 5 min linear gradient from 20% to 80% acetonitrile in 0.1% aqueous formic acid at a flow rate of 0.3 mL/min

https://doi.org/10.1021/acs.jnatprod.1c00946
J. Nat. Prod. XXXX, XXX, XXX−XXX

for the analysis of SBP-1 peptide. Cannabinoid separations were similar except that a 100 mm Waters Acquity UPLC BEH C_{18} column was used with a 1 min gradient from 50% to 75% acetonitrile followed by an 11 min gradient to 80% acetonitrile. The column was equilibrated to initial conditions for 1 min between analyses.

Ligands eluting from the column were detected using positive ion or negative ion electrospray mass spectrometry on the Q-ToF mass spectrometer at a resolving power of 30 000. The electrospray temperature was 300 °C, and voltages of 4.5 and −3.5 kV were used for positive or negative ion mode, respectively. The nitrogen gas flow rates for the electrospray ion source were 10 L/min for drying, 10 L/min for heating, and 3 L/min for nebulization. Data-dependent product ion tandem mass spectrometry was used such that mass spectra and product ion tandem mass spectra were acquired every 100 ms over the scan range of m/z 100−1200 and m/z 70−1200, respectively. For product ion MS/MS, the collision energy was 35 V with an energy spread of 17 V.

Following affinity selection, the UHPLC-MS chromatograms of each sample and corresponding negative control were compared using the metabolomics software Online XCMS (Scripps Research, La Jolla, CA, USA) to identify peaks enriched due to specific binding to the S1 protein.[43] High-resolution mass spectra for each enriched peak were processed using Shimadzu LabSolutions V5.2 software. Natural product ligands for which structures have been reported in the literature were identified by comparison with authentic standards based on their elemental compositions determined using high-resolution accurate mass measurements, tandem mass spectra, and UHPLC retention times.

Equilibrium Dissociation Constants. The affinity constants for the binding of active compounds to the spike protein S1 subunit were determined by rapid equilibrium dialysis. First, the optimum time for full equilibration of the RED device obtained from ThermoFisher (Waltham, MA, USA) was determined with each of the compounds by adding 1 μM spike protein in buffer (300 μL) to the protein chamber and adding blank phosphate-buffered saline, pH 7.2 (500 μL), to the buffer chamber. CBGA or CBDA was spiked into the protein chamber at a final concentration of 2.5 μM. During incubation at 37 °C on an orbital shaker at 200 rpm, aliquots (30 μL) were sampled from the sample and buffer chambers at 0.5, 1, 2, 3, 4, 5, 6, and 7 h, mixed with equal volumes of buffer, 300 μL of ice-cold 90% aqueous acetonitrile containing 0.1% formic acid, and 500 ng/mL d_4-daidzein (internal standard), vortex mixed, and incubated on ice for 1 h. After centrifugation at 18000*g* for 30 min, the supernatant was removed and ligand concentration was measured using UHPLC-MS/MS with selected reaction monitoring MS/MS and negative ion electrospray on a triple quadrupole mass spectrometer. For the measurement of CBGA, the selected reaction monitoring transitions were m/z 359 to m/z 341 (quantifier) and m/z 359 to m/z 315 (qualifier). For the measurement of CBDA, the selected reaction monitoring transitions were m/z 357 to m/z 339 (quantifier) and m/z 357 to m/z 245 (qualifier).

Next, the equilibrium dissociation constants of CBGA and CBDA were determined by incubating the spike protein S1 subunit with different concentrations of the ligands ranging from 0.05 to 500 μM in triplicate. After 5 h for CBGA or 4 h for CBDA, the concentrations of each ligand in the sample and buffer chambers were measured using UHPLC-MS/MS with a triple quadruple mass spectrometer as described above. Data analysis and fitting was carried out using Microsoft Excel (Seattle, WA, USA) and KaleidaGraph v4.1 (Reading, PA, USA).

Ligand Docking. The computational aided modeling of cannabinoids was carried out using AutoDock Vina (Scripps Research Institute, La Jolla, CA, USA).[44] The coordinates of the crystal structure of SARS-CoV-2 spike protein C-terminal domain were downloaded from the Protein Data Bank (PDB, ID number 6LZG).[45] The ChemDraw structures of the ligands were converted to .pdb files using Pymol. The protein data were loaded into the AutoDock Vina program, the search space was defined around the known orthosteric site, and the file was converted to .pdbqt. Similarly, the ligands were individually loaded and converted to .pdbqt files.

Pseudotyped Lentivirus Production. Pseudovirus was prepared as previously described.[46] 293T cells, seeded 1 day ahead with 2 million cells in 6 cm TC-treated dishes, were transfected with lentivirus packaging plasmids, SARS-CoV-2 S plasmid, and lzGreen reporter plasmid.[47] After transfection, cells were incubated at 37 °C for 60 h. Viral media were filtered with a 0.45 μm syringe filter and snap frozen in liquid nitrogen before storing at −80 °C. Virus stocks were titrated on 293T-ACE2 cells treated with 50 μL of 5 μg/mL Polybrene (Sigma-Aldrich, St. Louis, MO, USA). Titer was determined by fluorescence microscopy using a BZ-X700 all-in-one fluorescent microscope (Keyence, Itasca, IL, USA).

SARS-CoV-2 Virus Propagation. SARS-CoV-2 isolates USA/CA_CDC_5574/2020 [lineage B.1.1.7] (NR-54011), hCoV-19/South Africa/KRISP-K005325/2020 [lineage B.1.351] (NR-54009), and USA-WA1/2020 1 [lineage A] (NR-52281) were obtained through BEI Resources, diluted 1:10, and added onto 70% confluent Vero E6 cells. The cells were incubated for 1 h at 37 °C with rocking every 15 min. Additional media were added according to the manufacturer's recommended culture volume, and the cells were incubated for 72 h in a tissue culture incubator. Supernatant was centrifuged at 3000*g* for 5 min before aliquoting and freezing at −80 °C.

Pseudovirus Neutralization Assay. Pseudovirus neutralization was performed as previously described.[46] Briefly, 293T-ACE2 cells were seeded at 10 000 cells per well on tissue culture treated, poly lysine treated 96-well plates. Cells were grown overnight at 37 °C. LzGreen SARS-COV-2 S pseudotyped lentivirus was combined with 2-fold serial dilutions of CBDA and CBGA in DMSO or vehicle control. The virus−drug mixture was incubated at 37 °C for 1 h, after which virus was added to 293T-ACE2 treated with 5 μg/mL Polybrene. Cells were incubated with neutralized virus for 44 h, then fixed with 4% formaldehyde for 1 h at room temperature, incubated with DAPI for 10 min at room temperature, and imaged with a BZ-X700 all-in-one fluorescent microscope (Keyence, Itasca, IL, USA). Total areas of DAPI and GFP fluorescent signal were calculated using included microscope software (Keyence). To account for variability in cell count, green fluorescent signal was normalized to DAPI signal. For conditions with fewer DAPI foci, the modal value of DAPI signal for each set of replicates was used for normalization across that condition. Otherwise DMSO control values were used in normalization to manage DAPI inconsistency across replicates. IC_{50} values were calculated with combined replicate data in python using a three-parameter logistic model and plotted with the matplotlib data visualization library.

Focus Forming Assay for Live SARS-CoV-2. Focus forming assays were performed as previously described.[46,48] In brief, 96-well plates with subconfluent Vero E6 cells were infected with 50−100 virus titer per well of the original SARS-CoV-2 strain (WA-1/2020) or the variants (B.1.1.7 or B.1.351) in buffer containing CBDA or CBGA ranging from 100 to 0.625 μg/mL. DMSO was used as a vehicle control. The virus and drug mixtures were incubated for 1 h at 37 °C prior to addition to cells. The mixture was incubated with cells for 1 h at 37 °C before addition of overlay media (Opti-MEM, 2% FBS, 2% methylcellulose). Infection was allowed to proceed for 48 h; then plates were fixed for 1 h in 4% formaldehyde in phosphate-buffered saline (PBS). Cells were permeabilized (PBS, 0.1% saponin, 0.1% bovine serum albumin) for 30 min. Anti-SARS-CoV-2 spike protein alpaca immune serum was diluted 1:5000 in permeabilization buffer and incubated on plates overnight at 4 °C. Plates were washed three times with PBS with 0.1% Tween-20 (wash buffer) and incubated with antillama-HRP at 1:20 000 for 1 h at room temperature. Following three more washes in wash buffer, plates were developed with TrueBlue (Seracare) for 30 min before being imaged (CTL immunospot) and counted (Viridot).[49] Three separate dilution series were prepared for each experiment, each of which was used to prepare three technical replicates. IC_{50} values were calculated with combined replicate data in python using a three-parameter logistic model and plotted with the matplotlib data visualization library.

https://doi.org/10.1021/acs.jnatprod.1c00946
J. Nat. Prod. XXXX, XXX, XXX−XXX

Immunofluorescence. Vero E6 cells were seeded on 96-well glass-bottom optical plates coated with poly lysine solution; 20 000 cells were seeded per well. Cells were infected with SARS-CoV-2 as described above. At 24 h postinfection, cells were fixed with 4% paraformaldehyde in PBS for 1 h. The 96-well plates with SARS-CoV-2-infected Vero E6 cells were permeabilized with 2% bovine serum albumin and 0.1% Triton-X-100 in PBS. Transfected cells were incubated for 2 h at room temperature with a mouse anti-dsRNA antibody (Millipore Sigma) to stain SARS-CoV-2 replication sites in infected cells. Anti-mouse IgG AF555 conjugated secondary antibodies were added at 1:500 dilution for 1 h at RT (Invitrogen, Carlsbad, CA, USA). Confocal imaging was performed with a Zeiss LSM 980 using a 63× Plan-Achromatic 1.4 NA oil immersion objective. Images were processed with Zeiss Zen Blue software. Maximum intensity *z*-projections were prepared in Fiji.

■ ASSOCIATED CONTENT

Supporting Information

The Supporting Information is available free of charge at https://pubs.acs.org/doi/10.1021/acs.jnatprod.1c00946.

Tandem mass spectra of affinity selected CBDA, CBGA, and THCA-A and the corresponding standards; cytotoxicity of CBDA in mammalian cell lines (PDF)

■ AUTHOR INFORMATION

Corresponding Author

Richard B. van Breemen − *Linus Pauling Institute, Department of Pharmaceutical Sciences, College of Pharmacy, Oregon State University, Corvallis, Oregon 97331, United States*; orcid.org/0000-0003-2016-0063; Email: richard.vanbreemen@oregonstate.edu

Authors

Ruth N. Muchiri − *Linus Pauling Institute, Department of Pharmaceutical Sciences, College of Pharmacy, Oregon State University, Corvallis, Oregon 97331, United States*

Timothy A. Bates − *Molecular Microbiology & Immunology, Oregon Health & Science University, Portland, Oregon 97239, United States*

Jules B. Weinstein − *Molecular Microbiology & Immunology, Oregon Health & Science University, Portland, Oregon 97239, United States*

Hans C. Leier − *Molecular Microbiology & Immunology, Oregon Health & Science University, Portland, Oregon 97239, United States*

Scotland Farley − *Molecular Microbiology & Immunology, Oregon Health & Science University, Portland, Oregon 97239, United States*

Fikadu G. Tafesse − *Molecular Microbiology & Immunology, Oregon Health & Science University, Portland, Oregon 97239, United States*

Complete contact information is available at: https://pubs.acs.org/10.1021/acs.jnatprod.1c00946

Notes

The authors declare no competing financial interest.

■ ACKNOWLEDGMENTS

The authors thank Shimadzu Scientific Instruments for mass spectrometry support, the Global Hemp Innovation Center for supplying hemp extracts, and the EmerTher company for providing the Ni-NTA magnetic microbeads used in this investigation

■ REFERENCES

(1) https://www.worldometers.info/coronavirus/, accessed 15 Dec 2021.

(2) Centers for Disease Control and Prevention. https://www.cdc.gov/coronavirus/2019-ncov/science/science-briefs/scientific-brief-emerging-variants.html, accessed 15 Dec 2021.

(3) Walensky, R. P.; Walke, H. T.; Fauci, A. S. *JAMA* **2021**, *325*, 1037−1038.

(4) Tahir ul Qamar, M.; Alqahtani, S. M.; Alamri, M. A.; Chen, L. L. *J. Pharm. Anal.* **2020**, *10*, 313−319.

(5) Huang, C.; Wang, Y.; Li, X.; Ren, L.; Zhao, J.; Hu, Y.; Zhang, L.; Fan, G.; Xu, J.; Gu, X.; Cheng, Z.; Yu, T.; Xia, J.; Wei, Y.; Wu, W.; Xie, X.; Yin, W.; Li, H.; Liu, M.; Xiao, Y.; Gao, H.; Guo, L.; Xie, J.; Wang, G.; Jiang, R.; Gao, Z.; Jin, Q.; Wang, J.; Cao, B. *Lancet* **2020**, *395*, 497−506.

(6) Wu, F.; Zhao, S.; Yu, B.; Chen, Y.-M.; Wang, W.; Song, Z.-G.; Hu, Y.; Tao, Z.-W.; Tian, J.-H.; Pei, Y.-Y.; Yuan, M.-L.; Zhang, Y.-L.; Dai, F.-H.; Liu, Y.; Wang, Q.-M.; Zheng, J.-J.; Xu, L.; Holmes, E. C.; Zhang, Y.-Z. *Nature* **2020**, *579*, 265−269.

(7) Jiang, S.; Hillyer, C.; Du, L. *Trends Immunol.* **2020**, *41*, 355−359.

(8) Rabi, F. A.; Al Zoubi, M. S.; Kasasbeh, G. A.; Salameh, D. M.; Al-Nasser, A. D. *Pathogens* **2020**, *9*, 231.

(9) Tai, W.; He, L.; Zhang, X.; Pu, J.; Voronin, D.; Jiang, S.; Zhou, Y.; Du, L. *Cell. Mol. Immunol.* **2020**, *17*, 613−620.

(10) Turner, A. J. In *Protective Arm of the Renin Angiotensin System (RAS)*; Unger, T.; Steckelings, U. M.; dos Santos, R. A. S., Eds.; Elsevier: New York, 2015; pp 185−189.

(11) Hoffmann, M.; Kleine-Weber, H.; Schroeder, S.; Krüger, N.; Herrler, T.; Erichsen, S.; Schiergens, T. S.; Herrler, G.; Wu, N.-H.; Nitsche, A.; Müller, M. A.; Drosten, C.; Pöhlmann, S. *Cell.* **2020**, *181*, 271−280.

(12) Guo, Y.-R.; Cao, Q.-D.; Hong, Z.-S.; Tan, Y.-Y.; Chen, S.-D.; Jin, H.-J.; Tan, K.-S.; Wang, D.-Y.; Yan, Y. *Military Med. Res.* **2020**, *7*, 11.

(13) Du, L.; He, Y.; Zhou, Y.; Liu, S.; Zheng, B.-J.; Jiang, S. *Nat. Rev. Microbiol.* **2009**, *7*, 226−236.

(14) Sainz, B., Jr; Mossel, E. C.; Gallaher, W. R.; Wimley, W. C.; Peters, C. J.; Wilson, R. B.; Garry, R. F. *Virus Res.* **2006**, *120*, 146−155.

(15) Yuan, K.; Yi, L.; Chen, J.; Qu, X.; Qing, T.; Rao, X.; Jiang, P.; Hu, J.; Xiong, Z.; Nie, Y.; Shi, X.; Wang, W.; Ling, C.; Yin, X.; Fan, K.; Lai, L.; Ding, M.; Deng, H. *Biochem. Biophys. Res. Commun.* **2004**, *319*, 746−752.

(16) De Clercq, E. *J. Clin. Virol.* **2001**, *22*, 73−89.

(17) VanCompernolle, S. E.; Wiznycia, A. V.; Rush, J. R.; Dhanasekaran, M.; Baures, P. W.; Todd, S. C. *Virology* **2003**, *314*, 371−380.

(18) Cragg, G. M.; Newman, D. J. *Pure Appl. Chem.* **2005**, *77*, 7−24.

(19) Dias, D. A.; Urban, S.; Roessner, U. *Metabolites* **2012**, *2*, 303−336.

(20) von Nussbaum, F.; Brands, M.; Hinzen, B.; Weigand, S.; Habich, D. *Angew.Chem. Int. Ed.* **2006**, *45*, 5072−5129.

(21) Mishra, B. B.; Tiwari, V. K. *Eur. J. Med. Chem.* **2011**, *46*, 4769−4807.

(22) Newman, D. J.; Cragg, G. M. *J. Nat. Prod.* **2016**, *79*, 629−661.

(23) Kanjanasirirat, P.; Suksatu, A.; Manopwisedjaroen, S.; Munyoo, B.; Tuchinda, P.; Jearawuttanakul, K.; Seemakhan, S.; Charoensutthivarakul, S.; Wongtrakoongate, P.; Rangkasenee, N.; Pitiporn, S.; Waranuch, N.; Chabang, N.; Khemawoot, P.; Sa-Ngiamsuntorn, K.; Pewkliang, Y.; Thongsri, P.; Chutipongtanate, S.; Hongeng, S.; Borwornpinyo, S.; Thitithanyanont, A. *Sci. Rep.* **2020**, *10*, 19963.

(24) Muchiri, R. N.; van Breemen, R. B. *J. Mass Spectrom.* **2021**, *56*, e4647.

(25) van Breemen, R. B.; Huang, C. R.; Nikolic, D.; Woodbury, C. P.; Zhao, Y. Z.; Venton, D. L. *Anal. Chem.* **1997**, *69*, 2159−2164.

(26) Kaur, S.; McGuire, L.; Tang, D.; Dollinger, G.; Huebner, V. *J. Protein Chem.* **1997**, *16*, 505−511.

(27) Choi, Y.; van Breemen, R. B. *Combin. Chem. High Throughput Screen.* **2008**, *11*, 1−6.
(28) Rush, M. D.; Walker, E. M.; Prehna, G.; Burton, T.; van Breemen, R. B. *J. Am. Soc. Mass Spectrom.* **2017**, *28*, 479−448.
(29) van Breemen, R. B. *Curr. Trends Mass Spectrom.* **2020**, *18*, 18−25.
(30) Citti, C.; Linciano, P.; Panseri, S.; Vezzalini, F.; Forni, F.; Vandelli, M. A.; Cannazza, G. *Front. Plant Sci.* **2019**, *10*, 120.
(31) Hazekamp, A.; Fischedick, J. T.; Díez, M. L.; Lubbe, A.; Ruhaak, R. L. In *Comprehensive Natural Products II*; Mander, L.; Lui, H.-W.; Eds.; Elsevier: Oxford, UK, 2010; pp 1033−1084.
(32) Pellesi, L.; Licata, M.; Verri, P.; Vandelli, D.; Palazzoli, F.; Marchesi, F.; Cainazzo, M. M.; Pini, L. A.; Guerzoni, S. *Eur. J. Clin. Pharmacol.* **2018**, *74*, 1427−1436.
(33) https://www.fda.gov/news-events/press-announcements/fda-approves-first-drug-comprised-active-ingredient-derived-marijuana-treat-rare-severe-forms.
(34) Sun, Y.; Gu, C.; Liu, X.; Liang, W.; Yao, P.; Bolton, J. L.; van Breemen, R. B. *J. Am. Soc. Mass Spectrom.* **2005**, *16*, 271−279.
(35) Zhao, Y. Z.; van Breemen, R. B.; Nikolic, D.; Huang, C. R.; Woodbury, C. P.; Schilling, A.; Venton, D. L. *J. Med. Chem.* **1997**, *40*, 4006−4012.
(36) Liu, J.; Burdette, J. E.; Xu, H.; Gu, C.; van Breemen, R. B.; Bhat, K. P.; Booth, N.; Constantinou, A. I.; Pezzuto, J. M.; Fong, H. H.; Farnsworth, N. R.; Bolton, J. L. *J. Agric. Food Chem.* **2001**, *49*, 2472−2479.
(37) Rush, M. D.; Walker, E. M.; Burton, T.; van Breemen, R. B. *J. Nat. Prod.* **2016**, *79*, 2898−2902.
(38) Wang, Q.; Zhang, Y.; Wu, L.; Niu, S.; Song, C.; Zhang, Z.; Lu, G.; Qiao, C.; Hu, Y.; Yuen, K. Y.; Wang, Q.; Zhou, H.; Yan, J.; Qi, J. *Cell* **2020**, *181*, 894−904.
(39) Yi, C.; Sun, X.; Ye, J.; Ding, L.; Liu, M.; Yang, Z.; Lu, X.; Zhang, Y.; Ma, L.; Gu, W.; Qu, A.; Xu, J.; Shi, Z.; Ling, Z.; Sun, B. *Cell Mol. Immunol.* **2020**, *17*, 621−630.
(40) Tegally, H.; Wilkinson, E.; Giovanetti, M.; Iranzadeh, A.; Fonseca, V.; Giandhari, J.; Doolabh, D.; Pillay, S.; San, E. J.; Msomi, N.; Mlisana, K.; von Gottberg, A.; Walaza, S.; Allam, M.; Ismail, A.; Mohale, T.; Glass, A. J.; Engelbrecht, S.; Van Zyl, G.; Preiser, W.; Petruccione, F.; Sigal, A.; Hardie, D.; Marais, G.; Hsiao, N. Y.; Korsman, S.; Davies, M. A.; Tyers, L.; Mudau, I.; York, D.; Maslo, C.; Goedhals, D.; Abrahams, S.; Laguda-Akingba, O.; Alisoltani-Dehkordi, A.; Godzik, A.; Wibmer, C. K.; Sewell, B. T.; Lourenço, J.; Alcantara, L. C. J.; Kosakovsky Pond, S. L.; Weaver, S.; Martin, D.; Lessells, R. J.; Bhiman, J. N.; Williamson, C.; de Oliveira, T. *Nature* **2021**, *592*, 438−443.
(41) Wakshlag, J. J.; Schwark, W. S.; Deabold, K. A.; Talsma, B. N.; Cital, S.; Lyubimov, A.; Iqbal, A.; Zakharov, A. *Front. Vet. Sci.* **2020**, *7*, 505.
(42) Nguyen, L. C.; Yang, D.; Nicolaescu, V.; Best, T. J.; Ohtsuki, T.; Chen, S.-N.; Friesen, J. B.; Drayman, N.; Mohamed, A.; Dann, C.; Silva, D.; Gula, H.; Jones, K. A.; Millis, J. M.; Dickinson, B. C.; Tay, S.; Oakes, S. A.; Pauli, G. F.; Meltzer, D. O.; Randall, G.; Rosner, M. R. *bioRxiv* **2021**, 2021.03.10.432967.
(43) Tautenhahn, R.; Patti, G. J.; Rinehart, D.; Siuzdak, G. *Anal. Chem.* **2012**, *84*, 5035−5039.
(44) Trott, O.; Olson, A. J. *J. Comput. Chem.* **2009**, *31*, 455−461.
(45) Berman, H. M.; Westbrook, J.; Feng, Z.; Gilliland, G.; Bhat, T. N.; Weissig, H.; Shindyalov, I. N.; Bourne, P. E. *Nucleic Acids Res.* **2000**, *28*, 235−242.
(46) Bates, T. A.; Weinstein, J. B.; Farley, S.; Leier, H. C.; Messer, W. B.; Tafesse, F. G. *Cell Reports* **2021**, *34* (7), 108737.
(47) Crawford, K. H. D.; Eguia, R.; Dingens, A. S.; Loes, A. N.; Malone, K. D.; Wolf, C. R.; Chu, H. Y.; Tortorici, M. A.; Veesler, D.; Murphy, M.; Pettie, D.; King, N. P.; Balazs, A. B.; Bloom, J. D. *Viruses* **2020**, *12*, 513.
(48) Case, J. B.; Bailey, A. L.; Kim, A. S.; Chen, R. E.; Diamond, M. S. *Virology* **2020**, *548*, 39−48.
(49) Katzelnick, L. C.; Coello Escoto, A.; McElvany, B. D.; Chávez, C.; Salje, H.; Luo, W.; Rodriguez-Barraquer, I.; Jarman, R.; Durbin, A. P.; Diehl, S. A.; Smith, D. J.; Whitehead, S. S.; Cummings, D. A. T. *PLOS Neglect. Trop. Dis.* **2018**, *12*, e0006862.

https://doi.org/10.1021/acs.jnatprod.1c00946
J. Nat. Prod. XXXX, XXX, XXX−XXX